

Noise characterization of broadband fiber Cherenkov radiation as a visible-wavelength source for optical coherence tomography and two-photon fluorescence microscopy

Haohua Tu,^{1,*} Youbo Zhao,¹ Yuan Liu^{1,2}, Yuan-Zhi Liu,¹
and Stephen Boppart^{1,2}

¹*Biophotonics Imaging Laboratory, Beckman Institute for Advanced Science and Technology, University of Illinois at Urbana-Champaign, Urbana, IL 61801, USA*

²*Department of Bioengineering, University of Illinois at Urbana-Champaign, Urbana, IL 61801, USA*
[*htu@illinois.edu](mailto:htu@illinois.edu)

Abstract: Optical sources in the visible region immediately adjacent to the near-infrared biological optical window are preferred in imaging techniques such as spectroscopic optical coherence tomography of endogenous absorptive molecules and two-photon fluorescence microscopy of intrinsic fluorophores. However, existing sources based on fiber supercontinuum generation are known to have high relative intensity noise and low spectral coherence, which may degrade imaging performance. Here we compare the optical noise and pulse compressibility of three high-power fiber Cherenkov radiation sources developed recently, and evaluate their potential to replace the existing supercontinuum sources in these imaging techniques.

©2014 Optical Society of America

OCIS codes: (190.4370) Nonlinear optics, fibers; (180.1655) Coherence tomography; (180.4315) Nonlinear microscopy; (060.5295) Photonic crystal fibers.

References and links

1. U. Morgner, W. Drexler, F. X. Kärtner, X. D. Li, C. Pitris, E. P. Ippen, and J. G. Fujimoto, "Spectroscopic optical coherence tomography," *Opt. Lett.* **25**(2), 111–113 (2000).
2. F. E. Robles, C. Wilson, G. Grant, and A. Wax, "Molecular imaging true-colour spectroscopic optical coherence tomography," *Nat. Photonics* **5**(12), 744–747 (2011).
3. J. Yi, Q. Wei, W. Liu, V. Backman, and H. F. Zhang, "Visible-light optical coherence tomography for retinal oximetry," *Opt. Lett.* **38**(11), 1796–1798 (2013).
4. J. M. Dudley, G. Genty, and S. Coen, "Supercontinuum generation in photonic crystal fiber," *Rev. Mod. Phys.* **78**(4), 1135–1184 (2006).
5. Y. Wang, I. Tomov, J. S. Nelson, Z. Chen, H. Lim, and F. Wise, "Low-noise broadband light generation from optical fibers for use in high-resolution optical coherence tomography," *J. Opt. Soc. Am. A* **22**(8), 1492–1499 (2005).
6. W. R. Zipfel, R. M. Williams, R. Christie, A. Y. Nikitin, B. T. Hyman, and W. W. Webb, "Live tissue intrinsic emission microscopy using multiphoton-excited native fluorescence and second harmonic generation," *Proc. Natl. Acad. Sci. U.S.A.* **100**(12), 7075–7080 (2003).
7. C. Li, R. K. Pastila, C. Pitsillides, J. M. Runnels, M. Puoris'haag, D. Côté, and C. P. Lin, "Imaging leukocyte trafficking *in vivo* with two-photon-excited endogenous tryptophan fluorescence," *Opt. Express* **18**(2), 988–999 (2010).
8. J. Palero, V. Boer, J. Vijverberg, H. Gerritsen, and H. J. C. M. Sterenborg, "Short-wavelength two-photon excitation fluorescence microscopy of tryptophan with a photonic crystal fiber based light source," *Opt. Express* **13**(14), 5363–5368 (2005).
9. W. Zheng, D. Li, Y. Zeng, Y. Luo, and J. Y. Qu, "Two-photon excited hemoglobin fluorescence," *Biomed. Opt. Express* **2**(1), 71–79 (2011).
10. B. Schenkel, R. Paschotta, and U. Keller, "Pulse compression with supercontinuum generation in microstructure fibers," *J. Opt. Soc. Am. B* **22**(3), 687–693 (2005).
11. G. Chang, L.-J. Chen, and F. X. Kärtner, "Fiber-optic Cherenkov radiation in the few-cycle regime," *Opt. Express* **19**(7), 6635–6647 (2011).
12. H. Tu, J. Lægsgaard, R. Zhang, S. Tong, Y. Liu, and S. A. Boppart, "Bright broadband coherent fiber sources emitting strongly blue-shifted resonant dispersive wave pulses," *Opt. Express* **21**(20), 23188–23196 (2013).
13. M.-C. Chan, C.-H. Lien, J.-Y. Lu, and B.-H. Lyu, "High power NIR fiber-optic femtosecond Cherenkov radiation and its application on nonlinear light microscopy," *Opt. Express* **22**(8), 9498–9507 (2014).

14. H. Tu and S. A. Boppart, "Optical frequency up-conversion by supercontinuum-free widely-tunable fiber-optic Cherenkov radiation," *Opt. Express* **17**(12), 9858–9872 (2009).
15. E. Beaurepaire, L. Moreaux, F. Amblard, and J. Mertz, "Combined scanning optical coherence and two-photon-excited fluorescence microscopy," *Opt. Lett.* **24**(14), 969–971 (1999).
16. S. Tang, Y. Zhou, and M. J. Ju, "Multimodal optical imaging with multiphoton microscopy and optical coherence tomography," *J Biophotonics* **5**(5-6), 396–403 (2012).
17. C. Vinegoni, T. S. Ralston, W. Tan, W. Luo, D. L. Marks, and S. A. Boppart, "Integrated structural and functional optical imaging combining spectral-domain optical coherence and multiphoton microscopy," *Appl. Phys. Lett.* **88**(5), 053901 (2006).
18. B. W. Graf, E. J. Chaney, M. Marjanovic, S. G. Adie, M. De Lisio, M. C. Valero, M. D. Boppart, and S. A. Boppart, "Long-term time-lapse multimodal intravital imaging of regeneration and bone-marrow-derived cell dynamics in skin," *Technology* **01**(1), 8–19 (2013).
19. F. Lu and W. Knox, "Low noise wavelength conversion of femtosecond pulses with dispersion micro-managed holey fibers," *Opt. Express* **13**(20), 8172–8178 (2005).
20. F. Spöler, S. Kray, P. Grychtol, B. Hermes, J. Bornemann, M. Först, and H. Kurz, "Simultaneous dual-band ultra-high resolution optical coherence tomography," *Opt. Express* **15**(17), 10832–10841 (2007).
21. P. Cimala, J. Walther, M. Mehner, M. Cuevas, and E. Koch, "Simultaneous dual-band optical coherence tomography in the spectral domain for high resolution *in vivo* imaging," *Opt. Express* **17**(22), 19486–19500 (2009).
22. L. Liu, J. A. Gardecki, S. K. Nadkarni, J. D. Toussaint, Y. Yagi, B. E. Bouma, and G. J. Tearney, "Imaging the subcellular structure of human coronary atherosclerosis using micro-optical coherence tomography," *Nat. Med.* **17**(8), 1010–1014 (2011).
23. U. Möller, S. T. Sørensen, C. Jakobsen, J. Johansen, P. M. Moselund, C. L. Thomsen, and O. Bang, "Power dependence of supercontinuum noise in uniform and tapered PCFs," *Opt. Express* **20**(3), 2851–2857 (2012).
24. S. Shin, U. Sharma, H. Tu, W. Jung, and S. A. Boppart, "Characterization and analysis of relative intensity noise in broadband optical sources for optical coherence tomography," *IEEE Photon. Technol. Lett.* **22**(14), 1057–1059 (2010).
25. X. Liu, G. E. Villanueva, J. Lægsgaard, U. Möller, H. Tu, S. A. Boppart, and D. Turchinovich, "Low-noise operation of all-fiber femtosecond Cherenkov laser," *IEEE Photon. Technol. Lett.* **25**(9), 892–895 (2013).
26. B. Xu, J. M. Gunn, J. M. Dela Cruz, V. V. Lozovoy, and M. Dantus, "Quantitative investigation of the multiphoton intrapulse interference phase scan method for simultaneous phase measurement and compensation of femtosecond laser pulses," *J. Opt. Soc. Am. B* **23**(4), 750–759 (2006).
27. S. Bourquin, A. Aguirre, I. Hartl, P. Hsiung, T. Ko, J. Fujimoto, T. Birks, W. Wadsworth, U. Bünning, and D. Kopf, "Ultrahigh resolution real time OCT imaging using a compact femtosecond Nd:Glass laser and nonlinear fiber," *Opt. Express* **11**(24), 3290–3297 (2003).
28. A. Aguirre, N. Nishizawa, J. Fujimoto, W. Seitz, M. Lederer, and D. Kopf, "Continuum generation in a novel photonic crystal fiber for ultrahigh resolution optical coherence tomography at 800 nm and 1300 nm," *Opt. Express* **14**(3), 1145–1160 (2006).

1. Introduction

The lack of molecular contrast in standard optical coherence tomography (OCT) can be overcome by the spectroscopic OCT technique that is sensitive to optical absorption [1]. However, the absorption of endogenous molecules in biological samples occurs predominantly in the visible region (400–700 nm), not the near-infrared region (700–1400 nm) typically used in OCT, leading to the low sensitivity/contrast of these molecules. Due to the scarcity of dedicated OCT sources at visible wavelengths, recent studies have employed the use of spectrally filtered visible bands from commercial ps-pulse-induced supercontinuum (SC) lasers to image small concentration variations of hemoglobin in animal skin [2] and the eye [3]. Because the intrinsic relative intensity noise (RIN) of the SC from photonic crystal fibers [4] is known to degrade the OCT signal-to-noise ratio (SNR) [5], a natural question arises whether a low-noise alternative source is available. A seemingly independent but closely related situation is encountered in two-photon fluorescence microscopy (TPF), another widespread three-dimensional imaging technology with better spatial resolution but smaller fields-of-view. Because most fluorophores native to biological samples can only be (efficiently) two-photon excited around or below 700 nm [6], visible ultrafast pulses are often advantageous over conventional Ti:sapphire laser pulses (700–1000 nm) in label-free TPF applications such as cancer diagnostics and *in vivo* imaging. For example, 590-nm pulses from an optical parametric oscillator (OPO) were used to image leukocyte trafficking in mice through tryptophan fluorescence [7]. To avoid the expensive and bulky OPO, other studies developed customized fs-pulse-induced SC sources and filtered out the visible portion to image tryptophan [8] and hemoglobin [9]. No attempt has been made to compress the

spectrally filtered visible pulses, which have a typical duration of 600-800 fs (much longer than the transform-limited duration of 15-30 fs) [9], presumably due to the spectral incoherence (phase noise) [10] directly related to the high RIN of SC generation (amplitude noise) [4]. Thus, more efficiently excited TPF demands a cost-effective visible source that emits shorter compressible pulses. Recognizing the limitations of the SC sources in visible-light OCT and TPF, we identify three recently developed broadband high-power fiber Cherenkov radiation (CR) sources as promising alternatives [11–13] (Table 1).

Table 1. Comparison of visible fiber CR sources and the visible band of a typical fiber SC source.

Visible signal [reference]	CR [11]	CR-Laser-Quantum [11]	CR-Calmar [12]	“CR” [13]	CR-High-Q [13]	SC-Visible [4]
Pump laser (vendor)	Ti:Sa (home-built)	Ti:Sa (Taccor s, Laser Quantum)	Er: fiber (Mendocino, Calmar)	solid-state Yb (Mikan, Amplitude System)	Yb:KYW (Femto-Train, High-Q)	unknown all-fiber laser
Pump wavelength λ	830 nm	800 nm	1550 nm	1030 nm	1040 nm	1060 nm
FWHM pulse-width of pump (dechirped)	~10 fs	~15 fs (chirped)	80 fs	~250 fs	229 fs	~10 ps
Repetition rate f	1 GHz	1,000 GHz	50.2 MHz	54.77 MHz	80.2 MHz	25.1 MHz
Photonic crystal fiber (NKT Photonics)	NL-PM-750	NL-2.0-745-02	LMA-8	NL-3.7-975	NL-3.7-975	unknown
Fiber core diameter	1.8 μm	2.0 μm	8 μm	3.7 μm	3.7 μm	~5 μm
zero-dispersion wavelength	750 nm	745 nm	1157 nm	975 nm	975 nm	~1040 nm
Fiber length	10 cm	9 cm	9 cm	8.5 cm	9 cm	>2 m
β_2 at pump λ (fs^2/cm)	164	143	486	51	75	unknown
γ at pump λ (Wkm^{-1})	95	104	2.1	18	18	unknown
$\lambda/2$ plate controlling input polarization	used	used	not used	not used	used	not used
Free-space-to-fiber coupling efficiency	24%	47%	78%	no data	71%	all-fiber system
Fiber output power	190 mW	221 mW	1170 mW	650 mW	830 mW	5000 mW
Soliton order N	5.8	8.5	4.9	179	131	>500
Signal treatment		filtered			shaped	shaped
Signal central λ	540 nm	625 nm	620 nm	670 nm	638 nm	623 nm
Signal FWHM bandwidth	60 nm	45 nm	43 nm	90 nm	44 nm	45 nm
Signal average power	~50 mW	40 mW	85 mW	250 mW (<860 nm)	25 mW	N.A.
Signal averaged RIN (up to $f/2$)	no test	<-149.5 dB/Hz	-142.1 dB/Hz	no test	-123.9 dB/Hz	-112.3 dB/Hz
Signal pulse compressibility	no test	yes	yes	no test	no	no
Signal polarization ratio (typical)	no data	20:1	50:1	no data	5:1	random
Pump-CR conversion	20-30%	18%	7%	40%		N.A.
Long-term stability	no data	>30 hr	>300 hr	no data	no test	>100 hr

In contrast to the SC sources that spread narrowband pump pulses across a wide spectrum [4], these CR sources convert the pump pulses into phase-matched visible CR bands rather selectively [14]. Although the CR bands possess adequate average power (>40 mW) for OCT and TPF (Table 1), the corresponding RIN and/or pulse-compressibility/spectral-coherence (i.e., applicability to OCT and TPF) remains unknown. In this study, we aim to compare the optical noise of these sources, and correlate the measured RIN to the pulse compressibility in TPF and the SNR in OCT. The results may guide laser source engineering not only for dedicated visible-light TPF or OCT, but also for combined TPF/OCT imaging [15] that has demonstrated synergistic advantages [16–18].

2. Source reconstruction

Our CR source development/reconstruction adopts the typical setup to generate CR or SC by fs pulses [4,8–14]. The setup consists of a pump laser, an isolator, an aspheric lens to couple the laser to the fiber, a fiber stage to position the fiber, and collimating optics for fiber output. An optional half-wave plate may be used to control input polarization to maximize the CR output (Table 1). A fiber-coupled spectrometer (USB2000, Ocean Optics Inc.) is employed to record the CR (or SC) spectrum across the 400–1000 nm region. To reconstruct one reported CR source [11], we use a different photonic crystal fiber to produce a spectrally isolated and filterable CR (CR-LaserQuantum) that highly approximates our home-built CR source (CR-Calmar) [12] in central wavelength, bandwidth, and spectrum (Table 1) [Fig. 1(a),1(b)]. This allows direct comparison of their RIN [19]. Noticeably, the reconstructed CR source avoids the double-chirped-mirror that de-chirps the pump pulses after the isolator [11], leading to a more simplified setup with a tolerable decrease in CR conversion efficiency (Table 1).

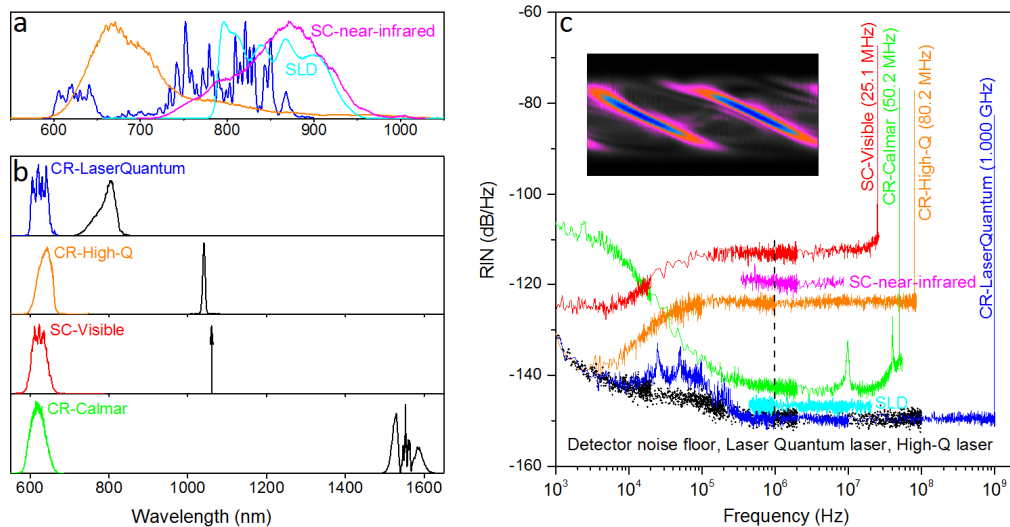


Fig. 1. (a) Measured optical spectra of raw CR-LaserQuantum (blue), raw CR-High-Q (orange), SC-near-infrared (magenta), and superluminescent diode (SLD) (cyan). (b) Measured optical spectra of filtered CR-LaserQuantum (blue), shaped CR-High-Q (orange), SC-Visible (red), CR-Calmar (green), and corresponding pump lasers (black). (c) Measured RIN spectra of SC-Visible (red), SC-near-infrared (magenta), shaped CR-High-Q (orange), CR-Calmar (green), SLD (cyan), filtered CR-LaserQuantum (blue), and the noise floor of detector or solid-state pump lasers (black); Inset: MIIPS trace of filtered CR-LaserQuantum indicative of pulse compressibility.

We also reconstruct another reported CR source [13] using a comparable pump laser (Table 1) [Fig. 1(a)]. To enable RIN comparison between the CR sources and the commercial SC sources employed in OCT applications [2,3,20–22], we acquired a prototype SC-laser (460–2000 nm) from a startup company that relies on the similar SC generation by mode-locked ~ 10 ps pulses (Table 1), and presumably has a similar RIN property as the commercial SC sources [4,23]. Using proper optics, we shape the CR source (CR-High-Q) and SC source (SC-Visible) to spectrally approximate the CR-Calmar source (Table 1) [Fig. 1(b)].

3. Noise measurements and discussions

The spectral similarity among the filtered/shaped CR and SC sources (Table 1) [Fig. 1(b)] permits direct comparison of their RIN [19]. Following our prior work [24,25], we detect each CR (or SC) signal and measure its RIN using a fast (1 ns rise time) Si detector (DET10A, Thorlabs, Inc.) connected to an electrical spectrum analyzer (HP 8561E, Agilent). The incident average optical power is attenuated to a constant unsaturated level (~ 2 mW) using a voltmeter (DC), thus avoiding any undesirable nonlinear response. The high-

frequency RIN of the signal has been reproducibly measured within ± 2 dB from 1 MHz to the pump laser repetition rate f (carrier frequency) [Fig. 1(c)] [19,23], corresponding to the amplified quantum noise [4,25] that may fundamentally limit the subsequent OCT and TPF applications. In contrast, the low-frequency (<1 MHz) RIN caused by technical laser noise can be removed by balanced detection (OCT) and intensity-modulation-lock-in-detection (TPF).

The RIN spectrum of the CR-Calmar source has peaks at 9.8 MHz and 40.4 MHz [Fig. 1(c)], which are also found in the RIN measurements of the pump laser using a 1550-nm-sensitive InGaAs detector (not shown). Thus, these non-white-noise features are caused by the Er: fiber pump laser itself. The RIN of the CR-LaserQuantum source falls on the noise floor of the Si detector, i.e., it is too low to be detected by our measurements. Using a more sensitive detector will not help because the noise floor of the Si detector is identical to that of the electrical spectrum analyzer. This low RIN implies the low RIN of the pump laser, which not surprisingly cannot be detected by the Si detector [Fig. 1(c)]. On the other hand, we cannot detect the RIN from the pump laser of the CR-High-Q source either [Fig. 1(c)], implying that the large RIN of CR-High-Q is due to the noise in fiber nonlinear wavelength conversion.

Since the pulse-to-pulse energy fluctuation of pulsed optical signal scales with the square root of integrated RIN from 1 MHz to the Nyquist frequency (i.e., $f/2$) [25], the energy fluctuation in a given short (<1 μ s) time (short-term power fluctuation σ) is proportional to the square root of the averaged RIN over the same frequency range (Table 1). Based on Fig. 1(c), σ of CR-High-Q, CR-Calmar, and CR-LaserQuantum can be calculated to be 5.8 dB, 14.9 dB, and >18.6 dB lower than that of the SC-Visible, respectively. It is rather surprising that CR-High-Q induced by a RIN-undetectable 1040-nm solid-state laser is 9.1 dB noisier in σ than CR-Calmar induced by a RIN-detectable fiber laser at a longer emitting wavelength of 1550 nm. In a fixed pump/fiber setup, nonlinearly converted components with larger wavelength offsets from the pump are noisier than those with smaller offsets [23]. To understand this discrepancy, we calculate the soliton order N of the CR or SC generation, according to the dispersion constant (β_2) and nonlinear coefficient (γ) of the photonic crystal fiber (Table 1) [4]. The soliton order to generate CR-High-Q exceeds 100, the regime known for high RIN and low spectral coherence [4]. Thus, the soliton order (and to a lesser degree, the noise of pump laser), not the wavelength offset from the pump [Fig. 1(b)], dictates the RIN and σ of CR signals in different pump/fiber combinations.

4. Applicability to TPF and OCT imaging

Temporal compression of the incident pulse can enhance TPF signal(s) without increasing the incident average power that may cause sample photo-damage. The most versatile method for ultrafast pulse compression is to use a programmable pulse shaper [10], which can be combined with a multiphoton intrapulse interference phase-scan (MIIPS) procedure [26] to test the compressibility (spectral coherence) of an unknown pulse. The spectral coherence of CR-Calmar has been confirmed by the characteristic MIIPS trace of two parallel lines, leading to transform-limited 17-fs pulses [12]. Similarly, we obtain a high-contrast MIIPS trace [Fig. 1(c), inset] and compress CR-LaserQuantum into transform-limited 17-fs pulses (Table 2). This is expected because the undetectably low RIN of CR-LaserQuantum [Fig. 1(c)] is directly associated with low phase noise and high spectral coherence [4]. The small but noticeable spectral modulation of CR-LaserQuantum [Fig. 1(a), 1(b)] deviates only 12% of the energy of the compressed pulses from the main peak to its sidebands, as found out by the autocorrelation trace measurement of the pulse shaper. Thus, this spectral modulation will not significantly affect the performance of TPF (or OCT) imaging.

However, under the similar experimental condition, we fail to obtain the characteristic MIIPS trace from CR-High-Q. The high RIN prohibits compression of CR-High-Q pulses, estimated to be ~ 600 fs (FWHM) by the generalized nonlinear Schrödinger equation [12] (Table 2). The high RIN and low spectral coherence indicates that CR-High-Q is more like a SC process than a CR process. Its high soliton order allows otherwise spectrally isolated CR

[11,12,14] to be mixed with (self- and cross-) phase modulations and four-wave mixing, leading to diminished spectral isolation from the pump [Fig. 1(a)]. Thus, the performance (signal strength and σ -related SNR) of CR-High-Q in TPF is comparable to that of the spectrally sliced fs-pulse-induced SC with ~ 700 fs pulse-widths [9]. Using these as the references, we compare several ~ 600 nm sources and find that CR-LaserQuantum and CR-Calmar are better alternatives to the OPO [7] (Table 2).

Table 2. Comparison of visible sources in TPF at given average power and scanning speed.

Visible source	CR-High-Q	OPO (~ 600 nm)	CR-LaserQuantum	CR-Calmar
FWHM pulse-width τ	600 fs (estimated)	200 fs (typical)	17 fs (compressed)	17 fs (compressed)
Repetition rate f	80.2 MHz	80 MHz (typical)	1.000 GHz	50.2 MHz
Signal strength $(\tau f)^{-1}$	0 dB (reference)	4.8 dB	4.5 dB	17.5 dB
SNR σ^2	0 dB (reference)	>25.6 dB (assumed)	>25.6 dB	18.2 dB

To avoid optical alignment effects in free-space OCT [2,3], a direct comparison of various sources requires coupling them to a visible-light fiber-based OCT system. With no such OCT system readily available, we instead examine the effect of source optical noise on the SNR of OCT using a near-infrared fiber-based spectral-domain OCT system (750-980 nm). The free-space beam of the SC-laser was coupled to the OCT system by an aspheric lens, while the wavelength-dependent single-mode fiber coupling resulted in a spectrum (SC-near-infrared) that highly approximates that of a fiber-coupled superluminescent diode (SLD) (widely used as a spectral-domain OCT source) [Fig. 1(a)]. Thus, direct comparison of the two sources can be performed by using the same incident average power to measure the SNR of otherwise identical OCT system. At 64 KHz spectrum acquisition rate, the measured SNR using SC-near-infrared (88 dB) was found to be 10 dB less than that using the SLD (98 dB). This can only be attributed to the 27 dB higher RIN of SC-near-infrared in comparison to the SLD ([Fig. 1(c)], note that SC-near-infrared has expectably lower RIN than SC-Visible [23]). Although commercial SC sources have become increasingly popular in OCT [2,3,20–22] and the RIN of some laboratory-built SC sources for OCT have been measured [5,27,28], the direct comparison of these sources to various SLDs in OCT performance evaluation has rarely been reported. Thus, this result calls for more systematic studies on how the source RIN properties quantitatively affect the SNR in OCT.

5. Conclusions and perspectives

We compare the applicability of three high-power visible fiber sources for TPF and OCT imaging. The high soliton order source [11] is accompanied by high RIN noise and low spectral coherence, which will limit its applications. The telecommunication-compatible portable CR source [12] has high spectral coherence useful for TPF, but may be limited by the detectable RIN in high-sensitivity (spectroscopic) OCT. The GHz CR source [13] has a lower TPF signal than the portable CR source, a disadvantage that may be partially compensated for by a higher SNR in high-speed TPF imaging. Also, the undetectably low RIN of the GHz CR source permits uncompromised OCT imaging. Moreover, because the ~ 15 fs pump laser of the GHz CR source is readily usable in near-infrared multimodal TPF/OCT [16], a visible/near-infrared dual-band OCT (TPF) can be built to more efficiently retrieve molecular absorption (fluorescence) contrast [20,21]. Finally, the compact maintenance-free pump laser of the GHz CR source allows potential widespread applications.

Acknowledgments

The authors are grateful to Daniel Jones for his technical support on one of the pump lasers (Taccors, Laser Quantum) used in this study. This research was supported by grants from the National Institutes of Health (R01 CA166309 and R01 EB013723).